

High-Performance Room-Light-Driven β -AgVO₃/mpg-C₃N₄ Core/Shell Photocatalyst Prepared by Mechanochemical Method

Hendrik Kosslick^{1,2*}, Yingyong Wang³, M. Farooq Ibad¹, Xiangyun Guo³, Matthias Lütgens⁴, Stefan Lochbrunner⁴, Marcus Frank⁵, Nguyen Quang Liem⁶, Axel Schulz^{1,2*}

¹Institute of Chemistry, University of Rostock, Rostock, Germany

²Leibniz-Institute for Catalysis at the University of Rostock, Rostock, Germany

³Institute of Coal Chemistry, State Key Laboratory of Coal Conversion, Chinese Academy of Sciences, Beijing, China

⁴Institute of Physics, University of Rostock, Rostock, Germany

⁵Electron Microscopic Center (EMZ), Institute of Pathology, University of Rostock, Rostock, Germany

⁶Institute of Materials Science, Vietnam Academy of Science and Technology, Ha Noi, Viet Nam

Email: *hendrik.kosslick@uni-rostock.de, *axel.schulz@uni-rostock.de

How to cite this paper: Kosslick, H., Wang, Y.Y., Ibad, M.F., Guo, X.Y., Lütgens, M., Lochbrunner, S., Frank, M., Liem, N.Q. and Schulz, A. (2021) High-Performance Room-Light-Driven β -AgVO₃/mpg-C₃N₄ Core/Shell Photocatalyst Prepared by Mechanochemical Method. *Advances in Chemical Engineering and Science*, 11, 290-315.

<https://doi.org/10.4236/aces.2021.114018>

Received: August 16, 2021

Accepted: October 17, 2021

Published: October 20, 2021

Copyright © 2021 by author(s) and Scientific Research Publishing Inc.

This work is licensed under the Creative

Commons Attribution International

License (CC BY 4.0).

<http://creativecommons.org/licenses/by/4.0/>



Open Access

Abstract

A new highly efficient, visible light active, silver vanadate/polymeric carbonitride “core/shell” photocatalyst was prepared mechano-chemically prepared by grinding mixtures of β -silver vanadate and mesoporous graphitic carbonitride. Besides the core/shell photocatalyst, β -silver vanadate/mesoporous polymeric carbonitride composites and supported mpg-C₃N₄@ β -silver vanadates were prepared. The materials were characterized by transmission electron microscopy (TEM), X-ray diffraction (XRD), nitrogen ad- and de-sorption, diffuse reflectance UV-Vis measurement (DRS), infrared spectroscopy, Raman microscopy, and time-resolved photoluminescence spectroscopy. The photocatalytic performance of the materials was investigated in the degradation of organics using pharmaceutical ibuprofen and 4-(isobutyl phenyl) propionic acid sodium salt as model compounds under batch conditions. Reaction intermediates were studied by electrospray ionization and time-of-flight mass spectrometry (ESI-TOF-MS). Additionally, the degree of mineralization was determined by total organic carbon TOC measurements. The core/shell photocatalyst has shown superior photocatalytic activity compared to the other prepared composites or supported photocatalysts as well as the single mpg-C₃N₄. Scavenger experiments showed that valence band holes and anionic superoxide radicals are the main active species in the photocatalytic process. TOC measurement confirmed the mineralization of the organic compound, which was in line with ESI-TOF-MS experiments. Time-resolved photoluminescence measurements indicated that charges generated in carbonitride mi-

grate via diffusive hopping and exhibit increased mobility in the case of the silver vanadate/polymeric carbonitride composite.

Keywords

Carbonitrides, Photocatalysis, Visible Light, Water Treatment, Mineralization, Core-Shell Catalyst, Silver Vanadate

1. Introduction

The sufficient supply of clean and drinking water for industrial, agricultural and human use, the supply of green, sustainable energy and protection of the environment from pollution are the main challenges to be solved in this century. The search for new materials and processes for more efficient use of energy resources and for remediation of water and the environment from pollution is of importance for solving these problems. The use of solar light as an ideal renewable energy source is believed to be the key to replace and save fossil energy resources with the efficient merits of the pollution less and non-exhaustible greenhouse gasses. Additionally, photocatalysis with solid-state semiconductors is of great potential for the development of new technologies addressing the above-mentioned concerns as hydrogen production from water and remediation of the environment from hazardous contaminations [1] [2] [3] [4]. Photocatalysis is a green technology, can be economically driven by sunlight, and is renewable, environmentally benign and safe [5].

A new emerging problem even in developed countries is the contamination of water by low concentrated but harmful pharmaceutical, hormones and endocrine-disrupting compounds. Photocatalysis with titania is an attractive method for water remediation, which can provide clean and drinking water [6] [7]. However, the titania photocatalysts still suffer from efficiency due to low quantum yield, low charge separation and the limited use of the spectral range of the sunlight. Attempts to improve the efficiency by increasing visible light response mainly by doping with metals and non-metals were performed. Despite the achieved success, the visible light response and overall efficiency are still limited [7] [8] [9] [10]. Therefore, the development of new visible light-active photocatalytic materials is still demanded.

Many attempts to discover new visible light active materials with the band gap energy in the range of the visible light (420 - 800 nm) were done. However, the band gap energy must be large enough to provide the valence band holes (h^+) and the conduction band electrons with appropriate potential required for water and pollutant oxidation and oxygen reduction to superoxide radicals ($O_2^{\cdot-}$). For example, TaON, Ta₃N₅ [11], CaBi₆O₁₀ [12], Sr_{0.25}Bi_{0.75}O_{1.36} [13], and Ag₃PO₄ [14], BiVO₄ [15] were shown to be visible light active in the oxidative photocatalytic degradation of organic pollutions.

Especially, silver vanadate materials, Ag_xV_yO_z were shown to be an active

p-type semiconductor with improved visible light activity due to its narrower band gap energy of 2.0 - 2.4 eV [16]-[24] compared to ZnO and TiO₂ which have higher band gap energies (~3.2 - 3.4 eV) [5] [25]. Recently, the influence of cation substitution in vanadates on the band gap was studied and compared to silver vanadate. Substitution with cerium led to a further decrease in the band gap energy [25].

Besides, large progress was achieved in the development of visible active graphitic carbonitrides, an n-type semiconductor, which has opened a new pathway for increasing efficiency. The influence of elemental doping or heterojunction on photocatalytic activity was extensively studied [26] [27] [28] [29] [30].

A couple of composite and core-shell catalysts [31] [32] was prepared and investigated, in order to further increase the activity of the mesoporous graphitic carbon nitrides mpg-C₃N₄. Different types of C₃N₄ composites consisting of e.g. core/shell Ag/C₃N₄ [33], binary C₃N₄/Ag₃VO₄ [34], Ag₃PO₄/C₃N₄ [35], AgX/C₃N₄ [36], C₃N₄/SmVO₄ [37], t-LaVO₄/C₃N₄, m-LaVO₄/C₃N₄ [38], GdVO₄/C₃N₄ [39], and ternary systems such as Ag/Ag₃PO₄/g-C₃N₄ [40], Ag/AgVO₃/C₃N₄ [41], g-C₃N₄/Ag/TiO₂ [42] with low carbon nitride loading but improved photocatalytic degradation activity were reported. Nevertheless, there is still a need for further improvement.

Only very few papers reported on silver vanadate carbon nitride composites, where the synthesis was carried out in solution via precipitation of silver vanadate on carbon nitride support which also resulted in side formation of metallic silver. Atomic silver in parallel takes part in photocatalysis as an electronic sink helping e⁻-h⁺ charge separation. In this paper, we report new β -AgVO₃/mpg-C₃N₄ core/shell and composite photocatalysts prepared by rapid solid-state mixing and thermal treatment. For comparative studies, β -AgVO₃/mpg-C₃N₄ composites were also prepared via co-precipitation in solution. The photocatalytic performance in the degradation of hazardous pharmaceutical contamination using ibuprofen (IBP) as a model compound was studied under sunlight equivalent UV-Vis and room light LED irradiation. The obtained composites have shown markedly improved activity compared with the single components. The β -AgVO₃/mpg-C₃N₄ core/shell photocatalyst displayed superior activity with 2 - 3 times increased activity compared to that of the composites. The atom efficiency regarding the precious metal content was significantly increased. The contribution of reactive oxygen species (ROS) and electron holes was investigated using scavenger molecules. Additionally, the charge migration and recombination in the composites after optical excitation were explored with time-resolved photoluminescence experiments.

2. Experimental Section

2.1. Materials and Synthesis

All of the chemicals were of analytical grade and used without further purification: Ibuprofen sodium salt (C₁₃H₁₇O₂Na, Sigma-Aldrich, 98%), ethylenediaminetetraacetic acid (C₁₀H₁₆N₂O₈, Sigma-Aldrich, 99%), *tert*-butanol (C₄H₁₀O, Sigma-Aldrich, 99%), double distilled water, silver nitrate (Sigma-Aldrich, 99%),

melamine (Fluka, 99%), ammonium vanadate (VEB Laborchemie Apolda, 98%), sulfuric acid (Fisher Scientific, 95%), Pluronic F68 (Sigma-Aldrich, 96%), Benzoquinone (Sigma-Aldrich, 98%). In the following, we describe the syntheses of the 4 kinds of samples to fulfill our study.

1) Synthesis of beta silver vanadate (β -AgVO₃). Nanorods of β -AgVO₃ were prepared by the precipitation route as reported before with some modifications [16] [23]. Typically, AgNO₃ (8.5 mmol, 1.443 g) and NH₄VO₃ (8.5 mmol, 0.994 g) were dissolved separately in 50 mL deionized water. Both solutions were simultaneously poured drop-wise from separate funnels into a 250 mL round bottom flask containing 30 mL deionized water in duration of 5 minutes, followed by stirring for 30 minutes. The formation of a bright yellow precipitate was noted. The yellow suspended solution was refluxed with vigorous stirring for 3 hours. A change in color from yellow to orange was noticed. The reaction mixture was aged for 14 hours followed by filtration with F4 filter. The collected precipitate was washed with 50 mL deionized water and ethanol respectively. Finally, the orange-colored solid (nanorods) was dried at room temperature for 5 hours and then at 110°C for 12 hours. In order to obtain silver vanadate powder, the material was calcined at 500°C for 3 hours. In the process of calcination, β -AgVO₃ melts at 476°C. After calcination β -AgVO₃ was obtained as a solid block and powdered with mortar and pestle.

2) Synthesis of mesoporous graphitic carbonitrides (mpg-C₃N₄). The mpg-C₃N₄ was prepared according to the reported procedure [43], however, using the amphiphilic block copolymer Pluronic F68 (EO₈₀PO₈₀EO₈₀, M = 8350, Aldrich) as a template. Typically, the mixture of melamine (5 g) and template Pluronic F68 (1.5 g) was refluxed in deionized water for 1 hour. To the cool solution, 3 mL of H₂SO₄ aqueous solution (H₂SO₄:H₂O = 1:1) was added. A white precipitate was obtained by filtration and dried at 80°C overnight. The obtained powder was heated up to 380°C with a rate of 5°C·min⁻¹, then to 600°C by 1.5°C·min⁻¹ in a quartz tube under flow of argon, and kept at this temperature for 4 hours. The resulting yellow powder was recalcined in a muffle furnace at 300°C for 3 hours in order to obtain the powdered sample.

3) Preparation of the β -AgVO₃/mpg-C₃N₄ composite. Suitable amounts of β -AgVO₃ and carbonitride were physically mixed together and grounded for 15 minutes in a mortar with the help of a pestle. The well-powdered mixture was calcined at 300°C for 3 hours in a closed crucible. The material was stored and used for further photoreactions. By this procedure, β -AgVO₃/mpg-C₃N₄ composites, containing 5%, 10%, 20%, 30%, 40%, 50% and 70% of β -AgVO₃, were prepared.

2.2. Characterization Methods

The crystallinity and structural phase of all used materials were characterized by powder X-ray diffraction (P-XRD) with the X-ray diffractometer STADI-P (STOE) and Ni-filtered Cu-K α ¹ radiation ($\lambda = 1.5418 \text{ \AA}$) in transmission. A curved Ge (111) monochromator (40 kV, 40 mA, linear PSD) was used. The

morphology and size of the catalysts were characterized on a LIBRA 120 transmission electron microscope (TEM) operated at 120 kV using carbon-coated copper grids. The porosity, specific surface area, pore volumes and pore sizes were determined by N_2 -adsorption and desorption isotherms using an automated device “Sorptomatic” (Porotec, ThermoScientific). The optoelectronic properties of the samples were studied with UV-Vis diffuse reflection measurements. The spectra were recorded on a fiber-coupled Araspee 2048 (Avantes) spectrometer equipped with an Avalight-DHS light source and a special reflection device suitable for measurements of solid materials. The band gap energies of the materials were obtained by a Tauc plot, in which for direct band gap $(h\nu\alpha)^2$ is plotted against the photon energy $h\nu$, where h is the Planck’s constant, ν the photon frequency, and α the absorbance at the considered frequency. The band gap energy is calculated using Schuster-Kubelka-Munk theory [44] [45] [46] [47] [48]. The FTIR spectra were recorded in the spectral range of 500 - 4000 cm^{-1} using a Nicolet 380 FT-IR spectrometer with a Smart Orbit ATR device. A Lab RAM HR 800 HORIBA Jobin Yvon Raman spectrometer equipped with an Olympus BX41 microscope with changeable lenses was used to record Raman spectra. The excitation of the samples was performed with a red laser (633 nm, 17 mW) or an infrared laser (785 nm, 100 mW) at ambient temperature. ESI-TOF-MS measurements were performed using an electrospray ionization mass spectrometer coupled with HPLC system 1200/ESI-TOF-MS 6210 (Agilent) to investigate qualitatively the formation of intermediates during photocatalytic treatment of the aqueous ibuprofen solution. The luminescence lifetimes and spectra were measured by a streak camera system (Streakscope C10627, Hamamatsu). The samples were illuminated with a frequency-doubled femtosecond pulse at 388 nm delivered from a Ti: Sapphire laser system (CPA 2001, Clark MXR). The sample powders were attached to glass substrates by a double-faced adhesive tape. The photon flux of the excitation was kept the same for all measurements to avoid intensity-dependent differences.

2.3. Photocatalytic Testing and Analysis

The photocatalytic abatement and adsorption of nonsteroidal anti-inflammatory drug IBP were studied under batch condition. The 250 mL glass beaker (batch reactor) containing 250 mL of a 10 ppm aqueous IBP solution and 10 mg of the catalyst was placed into a closed aluminum box equipped with a visible white light lamp (Toshiba 16 W, LED cold white light lamp), which is usually used for illumination of offices (rooms). For the UV-Vis illumination, four UV-Vis solarium lamps (Phillips) were used on the top with a total power of 60 W (4 lamps \times 15 W, Phillips). The irradiation intensity of the experimental setup was *ca.* 3.2 mW/cm^2 in the case of UV-Vis solarium lamp. These lamps mainly simulate the UV part of sunlight besides additional emission lines in the visible light range.

The solution was mixed magnetically during the photocatalytic experiments. For quantitative analysis of the irradiated solution, aliquots were taken at certain time intervals using a syringe equipped with a PTFE filter. Adsorption experi-

ments were carried out in the dark. The remaining IBP content in the samples was determined by the change of the intensity of IBP band at 320 nm using a UV-Vis spectrometer (Varian, Cary WinUV). After a particular interval of time, the amount of total organic carbon in aliquots was analyzed with a Shimadzu TOC-L CSH/CSN device.

3. Results and Discussion

3.1. Material Characterization

Structure. The XRD patterns of β -AgVO₃ and composite catalysts measured in the 2θ -range from 5° to 65° are shown **Figure 1**, respectively. The observed diffraction pattern of the prepared silver vanadate corresponds to the β -AgVO₃ phase (**Figure 1(a)**). The diffraction peaks were well indexed to monoclinic β -AgVO₃ (space group $C2/m$), with lattice constants of $a = 18.1060 \text{ \AA}$, $b = 3.5787 \text{ \AA}$ and $c = 8.0430 \text{ \AA}$, α and $\beta = 104.44^\circ$. These lattice constants correspond well to those given in the literature (COD: 96-150-9498), and no other patterns from possible impurities/modified lattices were detected. The rather narrow diffraction peaks indicated that the material was highly crystalline. No by-products such as metallic silver nanoparticles could be observed in the XRD pattern. Usually, the XRD pattern of mpg-C₃N₄ is characterized by a low intense reflection ca. $2\theta = 13^\circ$ and a high intense peak at ca. $2\theta = 27^\circ$. The XRD pattern of mpg-C₃N₄ of the β -AgVO₃/mpg-C₃N₄ composites is different from the reported ones [49] and show a broad and intense reflection at $12^\circ - 13^\circ$ and a low intense peak at ca. 27.5° . These reflections are attributed the (210) and to the (002) plane of mpg-C₃N₄, respectively [50]. The peak at 13.22° related to an in-plane structural packing motif of the tri-s-triazine units of the polymeric chain. The (210) reflection is sensitive to the structural order and its intensity increases with the crystallinity. The (002) peak is related out of plane motif of the polymeric layers. The highest intensity of the (002) peak is observed with the 20% β -AgVO₃/mpg-C₃N₄ core/shell catalyst material. It is not observed with 70% β -AgVO₃/mpg-C₃N₄ which contains a lot of bulky g-C₃N₄. It is concluded that the high intensity diffracted at 27° is related to the formation of ordered layers on the crystal surface of β -AgVO₃ nanorods, *i.e.* the formation of a “core/shell” structure. The parallel alignment of the mpg-C₃N₄ polymeric chains at the planar crystal faces of the β -AgVO₃ nanorods enhances the crystallinity.

Morphology and texture. The TEM images of the prepared β -AgVO₃ and β -AgVO₃/mpg-C₃N₄ composites are shown in **Figure 2**. The TEM images show that the silver vanadate consists of rods of the diameter 20 nm to 60 nm, with the length of submicron range. Mostly these rods are stacked together or agglomerated. The appearance of a composite particle depends strongly on the carbonitride content. Interestingly, with the 20% - 30% β -AgVO₃/C₃N₄ materials complete covering of the body of the β -AgVO₃ nanorods by carbonitride is observed, leading to the formation of the core/shell catalysts. **Figure 2(b)**, **Figure 2(c)** shows β -AgVO₃/mpg-C₃N₄ core/shell catalyst particles consisting of a *ca.* 25 nm

thick silver vanadate nanorods completely surrounded by a *ca.* 7 - 12 nm thick carbonitride shell (layer). In the case of the low and high silver vanadate content, 5% - 10% β -AgVO₃/C₃N₄, or ($\geq 40\%$ β -AgVO₃, the physical mixing and calcination led to agglomeration of the mpg-C₃N₄ component and attachment of the β -AgVO₃ particles, as typically found with agglomerated composites.

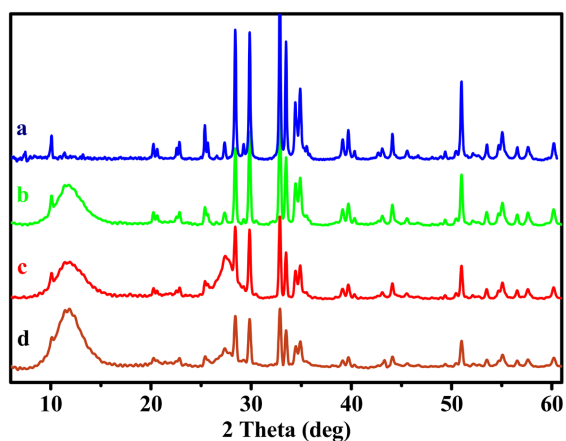


Figure 1. Powder XRD patterns of (a) β -AgVO₃, (b) 70% β -AgVO₃/mpg-C₃N₄, (c) 20% β -AgVO₃/mpg-C₃N₄, and (d) 5% β -AgVO₃/mpg-C₃N₄.

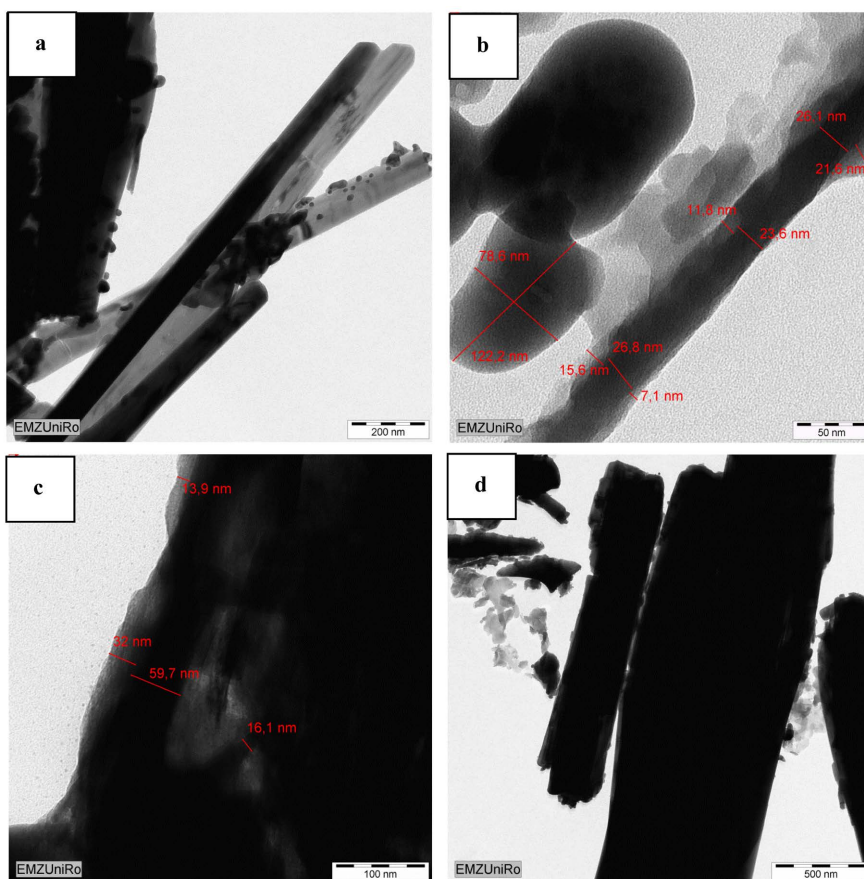


Figure 2. TEM images of (a) β -AgVO₃, (b) 20%, (c) 30%, and (d) 70% β -AgVO₃/mpg-C₃N₄ composites.

The textural properties of the mpg-C₃N₄, β -AgVO₃, and the composite samples were investigated by nitrogen adsorption-desorption measurements (Figure 3). The silver vanadate is nonporous showing only a very low nitrogen uptake at a relative pressure $p/p_0 \leq 0.3$ due to adsorption of nitrogen at the surface of the large silver vanadate nanorods (ca. 5 m²/g). In contrast, the mpg-C₃N₄ is mesoporous giving rise to a high nitrogen uptake at a high relative pressure of $p/p_0 > 0.8$. The specific surface area amounts to ca. 44.5 m²/g (BET). The specific surface area and pore volume are highest with catalysts containing 20% - 30% of silver vanadate. The mesoporosity is highest with the core/shell catalyst. At higher silver vanadate loading the specific surface area pore volume decreases down to ca. 19 m²/g and 0.24 cm³/g, respectively, with the 70% β -AgVO₃/C₃N₄ composite (Table 1).

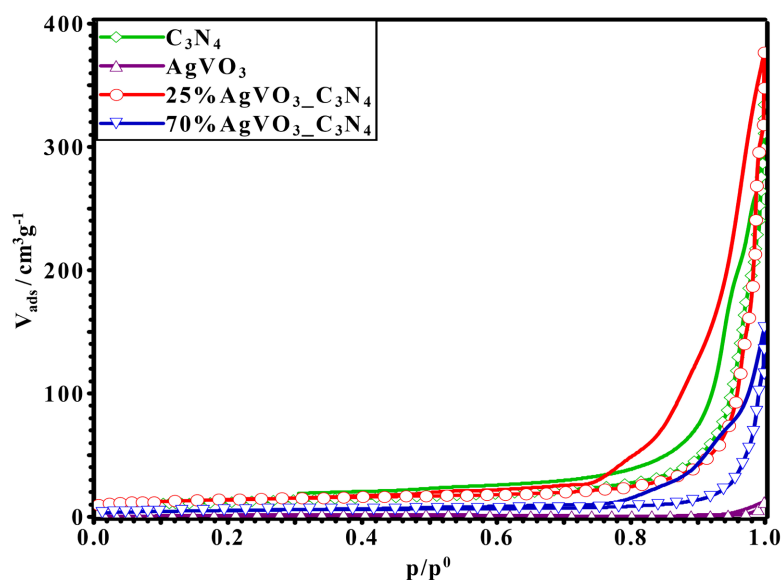


Figure 3. Nitrogen adsorption (assigned lines) and desorption (plain lines) isotherms of prepared β -AgVO₃, mpg-C₃N₄, and the corresponding β -AgVO₃/mpg-C₃N₄ composite and core/shell material.

Table 1. Specific surface areas, pore volumes and pored sizes of prepared β -AgVO₃, mpg-C₃N₄, and the corresponding β -AgVO₃/mpg-C₃N₄ composite and core/shell material.

Sample	Surface characteristics			
	BET surface (m ² /g)	Cumulative pore vol. (cm ³ /g)	Pore size maximum (nm)	Ads. Mean Pore diameter (nm)
β -AgVO ₃	5.4	0.20	1.99	19.33
mpg-C ₃ N ₄	44.5	0.50	30.99	39.5
Core shell 25% β -AgVO ₃ /mpg-C ₃ N ₄	50.6	0.58	15.47	27.33
Composite 70% β -AgVO ₃ /mpg-C ₃ N ₄	18.9	0.24	18.15	25.62

Vibrational spectroscopy. The FTIR-ATR spectra of β -AgVO₃/mpg-C₃N₄ and the corresponding β -AgVO₃/mpg-C₃N₄ composites in the mid-infrared range between 550 cm⁻¹ and 1600 cm⁻¹ are depicted in **Figure 4**. The FTIR-ATR spectrum of β -AgVO₃ shows characteristic bands for VO vibrations in the range between 400 - 1000 cm⁻¹ [51]. The strong and relative broad absorbance at *ca.* 793 cm⁻¹ can be assigned to symmetric V-O stretching vibrations [52]. Additionally, weak absorbances appear at *ca.* 671, 829, 857, 890, and 966 cm⁻¹ are in line with other observations [43]. The vibrational band at *ca.* 966 cm⁻¹ is assigned to the asymmetric stretching vibrations in the terminal vanadyl groups VO₃ [53]. The vibrational band at *ca.* 890 cm⁻¹ is ascribed to the V = O stretching mode. The stretching vibrations of both V-O and Ag-O-V give rise to the band observed at 857 cm⁻¹ [54]. The infrared spectra give no implication for the presence of impurities like vanadium pentoxide, for which vibrations should appear at *ca.* 1122, 833 or 617 cm⁻¹ arising from the V=O apex stretching of the pyramid [55]. Additionally, the absence of N-H, N-O and N=O vibrational bands above 3000 cm⁻¹ and in the range between 1400 - 1350 cm⁻¹, respectively, indicate that the prepared β -AgVO₃ contains no residual ammonia or nitrates.

The IR spectrum of the prepared and calcined mesoporous carbonitride shows main vibrational bands in the ranges between 2500 - 3600 cm⁻¹ and 800 - 1600 cm⁻¹. In the first region, a broad absorbance appears with the maximum centered at *ca.* 3160 cm⁻¹ that can be assigned to hydrogen-bonded N-H and O-H (residual water). The C≡N vibration, usually appearing at *ca.* 2100 cm⁻¹, was not observed. The complex spectrum observed in the range between 800 - 1600 cm⁻¹ is characteristic of the presence of C-N (800 - 1300 cm⁻¹) and C=N bonds (1500 - 1600 cm⁻¹). The intense band at 806 cm⁻¹ was assigned to C-C and C-N stretching vibrations. The FTIR-ATR spectra of the β -AgVO₃/mpg-C₃N₄ composites resemble the superposition of the spectrum of the β -AgVO₃ and mpg-C₃N₄ components indicating that no chemical reaction appears during the composite preparation. However, the relative transmittances of the vibrational bands of the two components have changed with the composition. Interestingly, the FTIR-ATR spectrum of the core/shell (20% β -AgVO₃/mpg-C₃N₄) material is dominated by the vibrational bands of the mpg-C₃N₄, arising at *ca.* 806 cm⁻¹. The strong vibrational band of the silver vanadate at *ca.* 793 cm⁻¹ nearly disappeared. This indicates that in the case of core/shell the silver vanadate nanorods are covered by mpg-C₃N₄ as typically expected for a core/shell catalyst (compare the TEM images (**Figure 2**). While in the case of a higher content of β -AgVO₃ the nanorods are not completely covered which gives rise to a low energy shoulder at the mpg-C₃N₄ mode (**Figures 4(c)-(d)**). In the case of the core-shell catalyst (**Figure 4(e)**) the 800 cm⁻¹ band is very narrow, which holds also for all the absorbances observed between 1200 - 1600 cm⁻¹ and between 2900 - 3400 cm⁻¹. The latter is resolved into three maxima arising at *ca.* 2900, 3200, and 3300 cm⁻¹. These findings point to a higher “crystallinity” or “layered arrangement” of the loaded mpg-C₃N₄ layer in the core/shell catalyst compared to the bulk mpg-C₃N₄ (**Figure 4**).

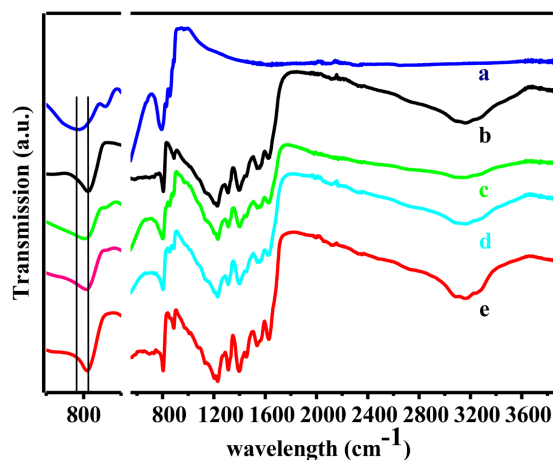


Figure 4. FTIR spectra of (a) β -AgVO₃, (b) β -mpg-C₃N₄, (c) 70% β -AgVO₃/mpg-C₃N₄, (d) 50% β -AgVO₃/mpg-C₃N₄, and (e) core shell 20% β -AgVO₃/mpg-C₃N₄.

Raman spectra of β -AgVO₃/mpg-C₃N₄ core/shell and composite materials, as well as the starting components, were recorded using a confocal microscope allowing the spatial-resolved measurements of samples. The complimentary Raman spectrum of a single bare β -AgVO₃ nanorod (Figure 5) is in line with reported spectral data, confirming the structural origin of the prepared material [56]. The strong Raman peak at 886 cm⁻¹ is assigned to vibrations of bridged O-V-O units [57] [58] [59]. The stretching mode of the VO₃ groups gives rise to a Raman peak at 845 cm⁻¹. The strong Raman peak at 810 cm⁻¹ can be assigned to the Ag-O-Ag stretching vibrations. The bridged V-O-V entities give rise to asymmetric and symmetric stretching vibrations appearing at 733 and 520 cm⁻¹, respectively. Additional Raman peaks located at 392, 339, 249, 173, and 132 cm⁻¹ are characteristic signatures of the β -AgVO₃ and can be referred to as the channel-structured β -silver vanadate [55]

The pure mpg-C₃N₄ shows a strong fluorescence. Single Raman peaks cannot be detected. Interestingly, the β -AgVO₃/mpg-C₃N₄ core/shell catalysts β -AgVO₃ shows no Raman lines. The C₃N₄ fluorescence completely overlaps the Raman spectrum of the β -AgVO₃. This finding is in line with a complete covering of the silver vanadate rods by carbon nitride layers. Uncovered β -AgVO₃ could not be detected indicating the formation of core/shell materials.

Light absorption and band structure. The optical properties of prepared β -AgVO₃, mpg-C₃N₄, and the corresponding β -AgVO₃/mpg-C₃N₄ composite core/shell catalysts were studied by Fourier-transform diffuse reflectance UV-Vis spectroscopy. The obtained spectra and derived Tauc plots are shown in Figure 6. The light absorption is extended to the visible light range for all the samples at ca. 600 nm. The light absorbance of silver vanadate β -AgVO₃ is red-shifted compared to carbonitride and silver vanadate/carbonitride samples. The absorption edge is well S-shaped and increases nearly linearly reaching a first absorbance maximum at ca. 440 nm. In contrast, the absorbance of the mpg-C₃N₄, and the corresponding β -AgVO₃/mpg-C₃N₄ composite catalysts increases in two

steps, a slow increase between 600 to 450 nm followed by a steep slope at <450 nm reaching the maximum absorbance at 380 nm. The shape of the spectra is very similar. The differences in absorbance are reflected in the Tauc plots.

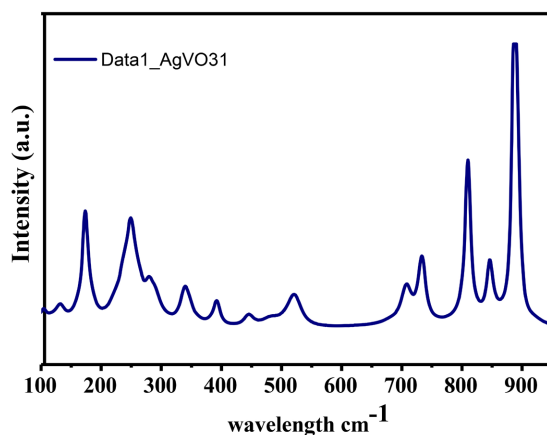


Figure 5. Raman spectrum of β -AgVO₃.

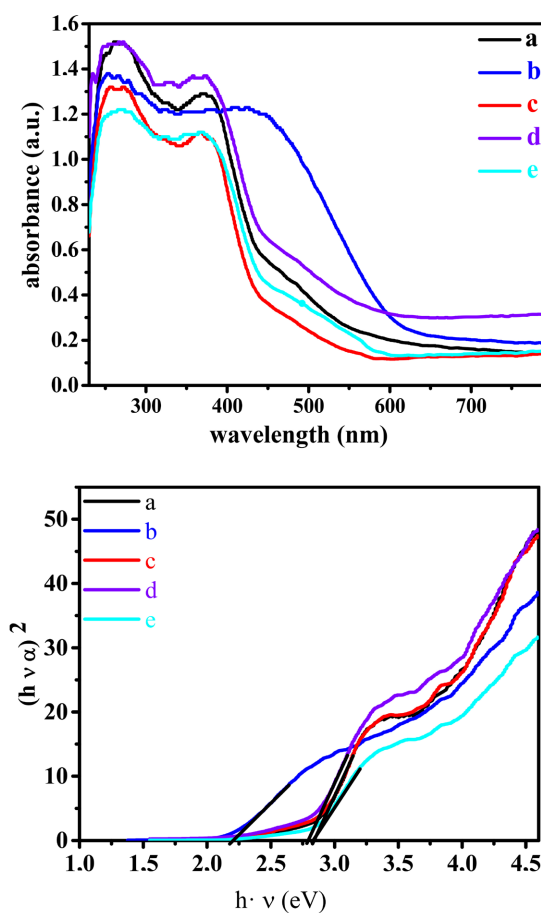


Figure 6. Diffuse reflectance UV-Vis spectra (top) and corresponding Tauc plots of $(h\nu\alpha)^2$ versus $h\nu$ (bottom) for (a) mpg-C₃N₄, (b) β -AgVO₃, and (c), (d), (e), for 20%, 30%, and 50% β -AgVO₃/mpg-C₃N₄.

The band gap of β -AgVO₃ calculated from Tauc plots, or obtained from the UV-Vis absorption edge is of lower energy (2.1 eV) compared to mpg-C₃N₄ (2.74 eV), the composites and the core-shell catalyst. The absorbance of the silver vanadate in the visible range is distinctly higher (Figure 6 left). The diffuse reflectance UV-Vis spectra of the corresponding β -AgVO₃/mpg-C₃N₄ composites are surprisingly dominated by the carbonitride and nearly coincide with it. The optical band gaps of the composites are close to that of the mpg-C₃N₄ and amount to ca. 2.69 - 2.74 eV (461 - 452 nm).

3.2. Photocatalysis

Photocatalytic performance. The photocatalytic performance of the β -AgVO₃, mpg-C₃N₄, and their composites and core-shell catalysts were checked in the abatement of ibuprofen in an aqueous solution at a very low concentration and low catalyst-to-substrate ratio. Photocatalytic degradation experiments were performed both, under UV-Vis and Visible light irradiation, with comparatively low intensity (room or sun (day) light equivalent). Please note that usually much higher catalyst loadings and irradiation intensity are applied with the commonly used 300 - 1000 W xenon, mercury or halogen lamps.

Irradiation with UV light. The absorption changes in UV-Vis spectra of ibuprofen solutions due to irradiation with UV and visible light are shown in Figure 7. For all β -AgVO₃/mpg-C₃N₄ composite catalysts, a decrease of the aromatic ring absorbance at 193.5 and 222 nm is observed due to the degradation or cleavage (opening) of the aromatic ring. At the same time, a new absorbance appears at ca. 260 nm. Its intensity increases and later decreases again with prolonged photocatalytic treatment. This band is assigned to the formation of reaction intermediates [6] [49] [60].

The relative abatement of ibuprofen vs. photocatalytic treatment time over different (5% - 70% β -AgVO₃/mpg-C₃N₄) composites compared to pure β -AgVO₃ and mpg-C₃N₄ are shown in Figure 8. Interestingly, an apparent increase in the abatement is observed in the first 30 min. of photocatalytic treatment, which is not observed in the dark. Obviously, it is due to the formation of reaction intermediates, partial oxidation products or radicals, which show a higher extinction coefficient than the starting IBP solution. Thereafter, a gradual decrease is observed due to the degradation of the IBP and intermediates. About 5% abatement of IBP is achieved after 8 h with the mpg-C₃N₄ alone. The addition of β -AgVO₃ (composites) leads to an improvement of the degradation to 10% and 22% with 5% and 10% β -AgVO₃ loading. Surprisingly, a boost of the activity is observed with the core/shell (20% β -AgVO₃/mpg-C₃N₄) material. Ca. 80% abatement is achieved after 8 h of photocatalytic treatment under UV-Vis irradiation. However, further enhancement of the β -AgVO₃ content to 70% leads again to a decrease of the degradation to ca. 55%. It is concluded that the exceptional high activity of the 20% β -AgVO₃/mpg-C₃N catalyst is related to the core/shell nature of this material, where the mpg-C₃N₄ is forming a thin (7 - 10 nm) shell around the β -AgVO₃ nanorods as evidenced by TEM. Pure β -AgVO₃ shows only

low activity with the formation of some partial oxidation products leading to an increase in the absorption band at *ca.* 193.5 nm according to UV-Vis spectroscopic studies.

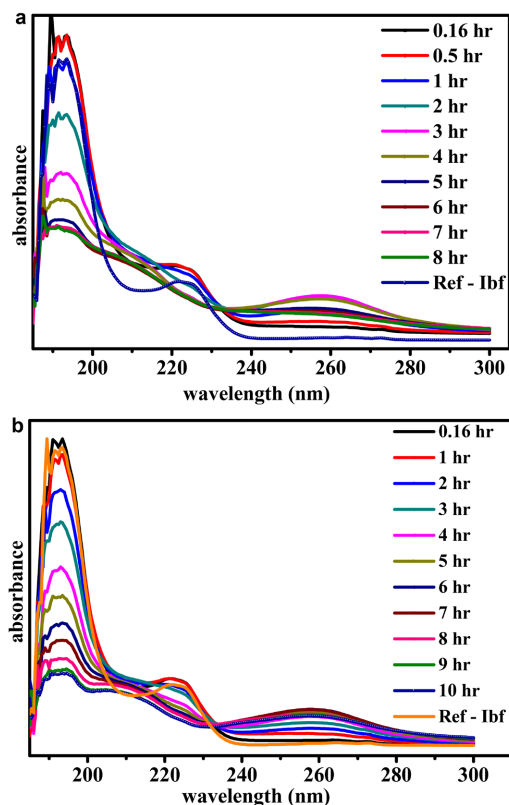


Figure 7. UV-Vis spectra of photocatalytic treated aqueous IBP solution in dependence of time, over β -AgVO₃/mpg-C₃N₄ core/shell photocatalyst using (a) UV-Vis, (b) Visible light; (40 mg/L catalysts, 250 mL of 10 ppm IBP. Solution, Irradiation: 60W UV-Vis light or 16W LED room light lamp).

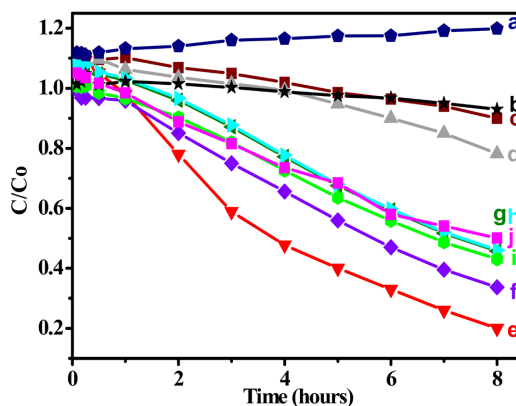


Figure 8. Relative abatement of IBP during the course of photocatalytic treatment under UV-Vis irradiation over (a) β -AgVO₃, (b) mpg-C₃N₄, and β -AgVO₃/mpg-C₃N₄ composites containing, (c) 5%, (d) 10%, (e) 20%, (f) 30%, (g) 40%, (h) 50% and (i) 70% of silver vanadate.

Irradiation with visible room light. The degradation behaviour of the β -AgVO₃/mpg-C₃N₄ composite catalysts under room light visible irradiation is similar to the results obtained under UV-Vis solarium light irradiation (Figure 9). The photocatalytic degradation of the IBP proceeds somewhat slower. Again, the core/shell catalyst (20% β -AgVO₃/mpg-C₃N₄) showed superior activity. Namely ca. 80% of ibuprofen degradation was achieved after 13 h. Again, the formation of reaction intermediates was observed in UV-Vis spectra of the reaction solution at the beginning of the treatment giving rise to absorbance at ca. 260 nm. The other composites showed a distinctly lower activity with up to ca. 30% of degradation over 30%, 50% and 70% β -AgVO₃/mpg-C₃N₄ composites. Hence, the difference in the photocatalytic degradation activity between the core/shell catalyst is much more pronounced under room light than under UV irradiation. In summary, the catalyst 20% β -AgVO₃/mpg-C₃N₄ shows the best performance resulting from the core/shell structure.

As under UV-Vis irradiation, an increase of the pollutant absorbance was observed in the first two hours of treatment. This effect is highest for the less active catalyst β -AgVO₃ and is assigned to the formation of intermediate partial oxidation products like hydroxylated side chains and benzene products with increased extinction coefficients. The composite catalyst 5% β -AgVO₃/mpg-C₃N₄ showed the same effect while it was not observed with the active core-shell catalyst confirming the improved oxidation power of these catalysts. Both, irradiation with sunlight UV as well as with room light, cause similar changes in the UV-Vis spectra of the irradiated solution indicating that there is no difference in the degradation mechanism between the two light sources.

Finally, a 20-time increase of photocatalytic activity was noted with the core/shell catalyst compared to the single mpg-C₃N₄, while the increase is markedly lower with the composites (ca. 9 times) or hybrid systems [61]. Compared to silver vanadate the activity in the degradation of ibuprofen is enhanced almost by 100 times under sunlight equivalent UV and Visible light.

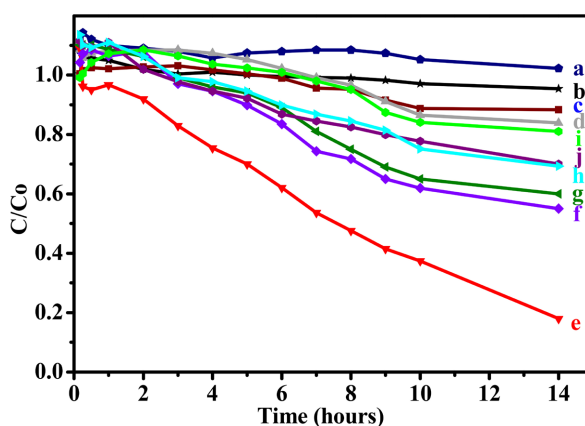


Figure 9. Relative abatement of IBP during the course of photocatalytic treatment under visible room light irradiation over (a) β -AgVO₃, (b) mpg-C₃N₄, and β -AgVO₃/mpg-C₃N₄ composites containing (c) 5%, (d) 10%, (e) 20%, (f) 30%, (g) 40%, (h) 50% and (i) 70% of silver vanadate.

Mineralization. The TOC measurements of the photocatalytic solution show that the photocatalytic treatment over the core/shell catalyst leads to ~75% degradation (mineralization) of the IBP (Figure 10). The determined degradation is in line with the UV-Vis spectroscopic results. However, the degree of mineralization is lower than the abatement determined by UV-Vis spectroscopy. The latter is sensitive to the aromatic ring opening only and not directly related to the complete degradation of the molecules to carbon dioxide and water.

In the case of Visible light irradiation, TOC results show only a minor change in the carbon content in the first 3 h of photocatalytic treatment. This finding is in line with the UV-Vis spectra of room light treated solution which indicates the formation of partial oxidation products, e.g. by hydroxylation of the side chain which causes no loss of carbon. Over pure AgVO_3 and mpg- C_3N_4 ibuprofen is nearly not mineralized.

Reaction intermediates. ESI-TOF-MS measurements in the positive and negative mode were carried out to study the formation of reaction intermediates during the course of photocatalytic treatment using UV and Visible light irradiation. The negative ESI-TOF-MS spectrum of the starting solution shows the $[\text{M-H}]^-$ mass peak of the IBP at *ca.* $m = 205$ and by-product mass peaks (likely partial oxidation product of IBP) at *ca.* $m = 273, 263, 301$ and others. Additionally, mass peaks at *ca.* $m = 433, 501$ and 661 were assigned to IBP sodium salt dimers and trimers. Already after 10 min. of treatment with UV-Vis or room light irradiation the appearance of the ESI-TOF-MS spectra markedly changed. A couple of new mass peaks assigned to partial oxidation and higher molecular mass polymerization products appeared. The intensity of the mass peaks generally decreases with prolonged treatment time. The composition of the photocatalytic treated solution regarding the nature of contained species was not markedly changed with only some exceptions. The species with the mass peak $m = 112$ and in part $m = 273$ (measured in negative mode) and $m = 90.9$ and $m = 130$ (positive mode) are more recalcitrant against the photocatalytic treatment. Overall, the core/shell catalyst leads to more efficient degradation of the organics. After 8 h UV or 13 h visible light irradiation, respectively, substantial degradation of the IBP is evidenced by the negative and positive ESI-TOF-MS spectra, generally confirming the UV spectroscopic and TOC finding of high degradation (80% and 75% respectively). The intensity of the ESI-TOF-MS signals decreases after photocatalytic treatment distinctly after 8h of treatment.

Reactive species. Generally, a couple of active species like reductive conduction band electrons (e^-) and oxidative valance band holes (h^+), hydroxyl radicals (OH^\bullet), hydroperoxyl radicals ($^{\bullet}\text{OOH}$) and oxygen radical anions ($\text{O}_2^{\bullet-}$) can be involved in the photocatalytic degradation process, but the contribution is different from catalyst to catalyst. We have studied the photocatalytic degradation in the presence of the h^+ , OH^\bullet , $^{\bullet}\text{OOH}$ scavengers, EDTA, t-butanol and benzoquinone [62] [63] [64] respectively, in order to differentiate between the active species involved with the core/shell and composite catalysts (Figure 11).

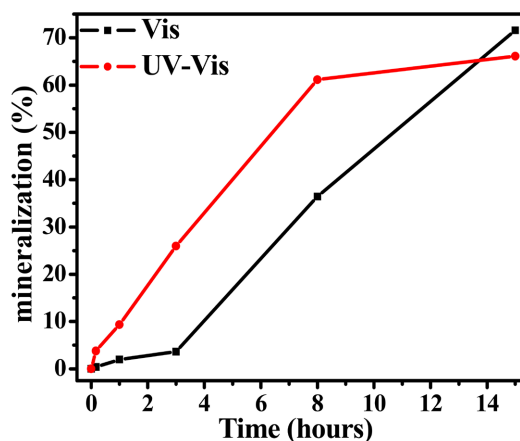


Figure 10. TOC plot of the mineralization of IBP under UV-Vis and Visible light irradiation over the core/shell (20% β -AgVO₃/mpg-C₃N₄) catalyst (catalyst loading 40 mg/L, reaction solution volume 250 mL containing 10 ppm IBP).

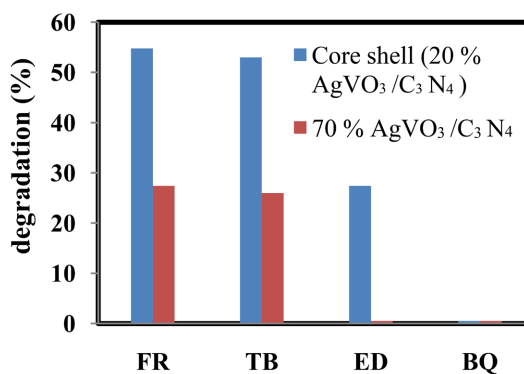


Figure 11. Impact of scavengers on the relative photocatalytic abatement of ibuprofen over 20% β -AgVO₃/mpg-C₃N₄ core/shell catalyst (blue) and 70% β -AgVO₃/mpg-C₃N₄ composite (red) under UV-Vis light irradiation. Without scavenger (Fr), 1.0 mL t-butanol (TB), 1.46 mg EDTA (ED), 1.46 mg Benzoquinone (BQ). Conditions: 10 ppm, 250 mL, IBP in water over photocatalyst 40 mg/L using 60 W UV-Vis light radiation for 4 hours.

Generally, the addition of t-butanol as OH[•] scavenger to the reaction chamber had no effect on the photocatalytic degradation, in 70% AgVO₃/mpg-C₃N₄ and core/shell photocatalyst. A pronounced effect of the hole-scavengers was observed in the case of the 70% AgVO₃/mpg-C₃N₄ composite catalyst. The addition of EDTA retarded the degradation of the ibuprofen (Figure 11 ED). The increase of the absorbance ~260 nm of solution related to intermediates in the UV-Vis spectra of the solution indicated the preferential formation of partially oxidized products of ibuprofen. In contrast in case of the core/shell catalyst, (20% AgVO₃/mpg-C₃N₄), the addition of the same amount of EDTA diminished the degradation of IBP only by ca. 27%. More EDTA was needed to further diminish the photocatalytic activity. That means, more holes h⁺ are available with the core/shell compared to the composite material. A strong decrease in the de-

gradation was observed after the addition of benzoquinone for both the catalysts indicating the pronounced contribution of $O_2^{\cdot-}$ or $\cdot OOH$ radicals in the photocatalytic degradation process (Figure 11 BQ).

Similar results were obtained with visible light. However, the degradation with visible light proceeds slower. Obviously, the excitation of valence band electrons is more efficient with UV light, because electrons from all energetic levels of the valence band can be excited to different states of the conduction band. In contrast, the restricted energy of the visible light (band gap) allows only exciting high-level valence band electrons to the lower energetic state of the conduction band.

In summary, the results show that the species involved in the photocatalytic degradation of organics are in general the same for both types of catalysts, the composites and the core-shell catalyst, but the activities differ substantially. The markedly higher photocatalytic degradation activity of the core/shell catalyst compared to that of the coupled β -AgVO₃/mpg-C₃N₄ composites is assigned to enhanced charge separation. Due to the complete surrounding of the silver vanadate core by a mesoporous graphitic carbon shell the recombination via internal recombination and recombination of surface excitons ($e-h^+$ pairs) at the silver vanadate is diminished. The charge separation of electron-hole pairs, and finally the photocatalytic activity, is improved. Besides, additional factors improve the performance of the core/shell catalyst: the enhanced specific surface area and the mesoporosity of graphitic carbonitride/silver vanadate catalysts can facilitate the photocatalytic degradation by increased the number and accessibility of surface sites. It is noticed that the small thickness of the shell of 7 - 11 nm facilitates the migration of excitons formed in the bulk to the surface.

The degradation of IBP reaches up to 80% over the pure core/shell catalyst in 8 hours and only *ca.* 50% over the composite catalyst even when the silver vanadate content of the composite was much higher. The core/shell catalyst is superior to the corresponding composites especially considering the atom efficiency based on the noble silver under UV as well as under visible light. In both cases valence band holes and conduction band hydroperoxyl radicals are the predominant species in the photocatalytic degradation, however, the effective number of holes is *ca.* doubled in the case of the core/shell catalyst according to the above-discussed reasons.

3.3. Charge Transport and Possible Mechanism

Photoluminescence measurements were carried out in order to get a deeper insight into the charge transfer processes. The charge migration mechanism of the β -AgVO₃/mpg-C₃N₄ composite catalyst was investigated by time-resolved photoluminescence spectroscopy. After optical excitation of the mpg-C₃N₄-composite at 388 nm, a broad fluorescence spectrum and non-exponential fluorescence decay within several nanoseconds were observed. This temporal behavior was already observed in several investigations of pure mpg-C₃N₄ [65] [66]. The results of the

time-resolved luminescence measurements are shown in **Figure 12**. The spectral shape of the fluorescence does not change with time indicating that the fluorescence originates always from the same species. For analyzing the time dependence, we used the wavelength integrated fluorescence signals are shown in **Figure 12 mid**, which were obtained by combining measurements of several time windows. In general, the curves show similar behavior, independent of the β -AgVO₃ content. This is a clear hint that the observed dynamics are dominated by processes occurring within the carbon nitride. Merschjann *et al.* [67] developed a hopping model, which seems to be valid not only for pure mpg-C₃N₄ but also for the β -AgVO₃/mpg-C₃N₄ composites investigated here. This model is based on a very fast charge separation after optical excitation, which is beyond

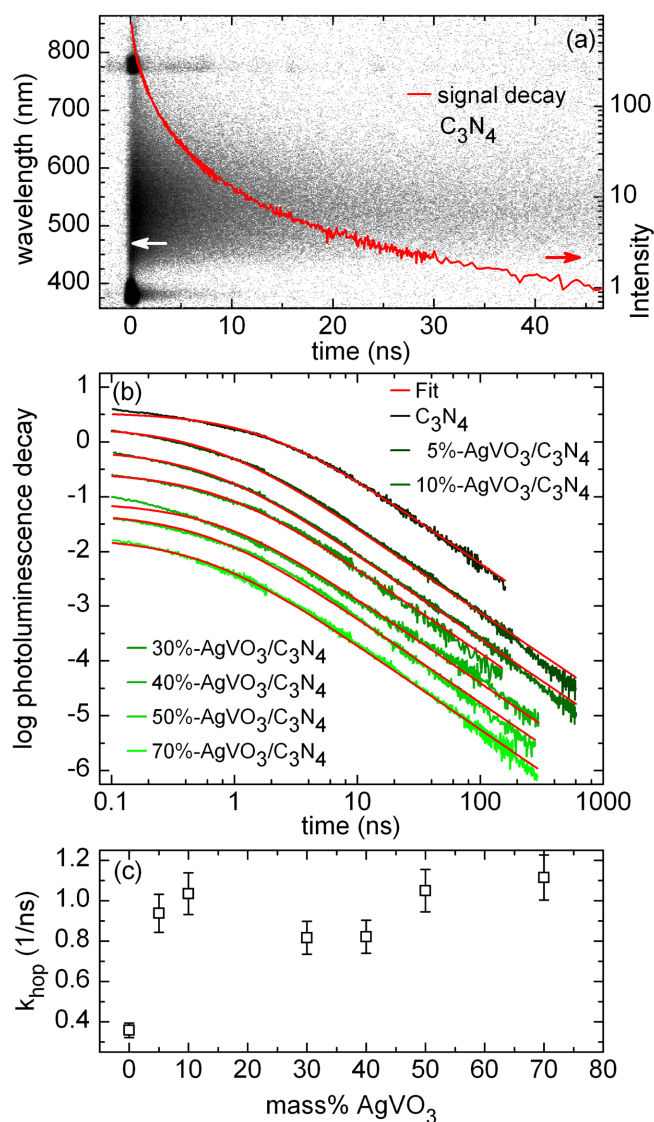


Figure 12. Scheme of charge transfer and photocatalytic degradation of organics over β -AgVO₃/mpg-C₃N₄ core-shell catalyst. AgVO₃ rods (gold-orange) covered by ordered arranged mpg-C₃N₄ sheets (wheat brown).

the time resolution of the performed time-resolved fluorescence experiment. Afterward electrons and holes migrate in a one-dimensional random walk motion from one lattice site to another. The motion most likely takes place perpendicular to the carbonitride sheets *i.e.* the carrier is hopping from plane to plane. If the charges meet again the hole and electron recombine leading to a singlet or triplet exciton which seems to decay rapidly. The singlet excitons can radiate during their short lifetime resulting in the detected fluorescence. The described geminate recombination process results in a charge carrier density n which obeys the rate equation

$$\frac{d}{dt}n(t) = -\gamma_{\text{gem}}(t, D)n(t) \quad (1)$$

The geminate recombination coefficient γ_{gem} depends thereby on the time and the dimensionality of the motion. For a one-dimensional motion, the geminate coefficient reads

$$\gamma_{\text{gem}} = \frac{1}{2}k_{\text{rec}}k_{\text{hop}} \left[1 + (3/2)^{1/3} k_{\text{hop}} t \right]^{-3/2} / (k_{\text{rec}} + k_{\text{hop}}) \quad (2)$$

with the recombination rate k_{rec} and the hopping rate k_{hop} . Solving this equation for $k_{\text{rec}} \gg k_{\text{hop}}$ yields the time depended on photon emission flux [68].

$$\Theta(t) = c_0 \exp \left\{ \frac{\left[\left(1 + (3/2)^{1/3} k_{\text{hop}} t \right)^{-1/2} \right]}{(3/2)^{1/3}} \right\} \times \frac{k_{\text{hop}}}{\left(1 + (3/2)^{1/3} k_{\text{hop}} t \right)^{3/2}}. \quad (3)$$

Possible mechanism. The most active species in mpg-C₃N₄ materials are electron-holes and superoxide radical anions. As shown by the scavenger studies above, the number of holes of the core-shell catalyst is doubled compared to the most active other composite catalysts. Both structure and morphology of the core-shell and composite materials are qualitatively different. The core/shell catalyst (**Figure 13**) is superior because the silver vanadate nanorods are 1) completely covered by mpg-C₃N₄; 2) mpg-C₃N₄ forms thin layers with the 2D plains of the mpg-C₃N₄ sheets are parallel aligned to the flat surface facets of the β -AgVO₃ nanorods; and 3) compared to the bulky C₃N₄ composite particles, in the core/shell, the mpg-C₃N₄ polymers planes are arranged layer by layer and exposed to the outer surface [69]. The improved long-range order of the optical tri-s-triazine units in the 2-dimensional mesoscopic polymer matrix enhances markedly the charge carrier mobility [70]. The mesoporous structure is good to promote the transportation of charge carriers from/to the β -AgVO₃ core nanorod through the shell to discharge the core, to make it ready again for the light absorption.

This special architecture diminishes the surface recombination of e-h pairs of β -AgVO₃, and partially on the mpg-C₃N₄ at the interface, and improves the charge separation of mpg-C₃N₄ e-h pairs in the bulky layer. The parallel

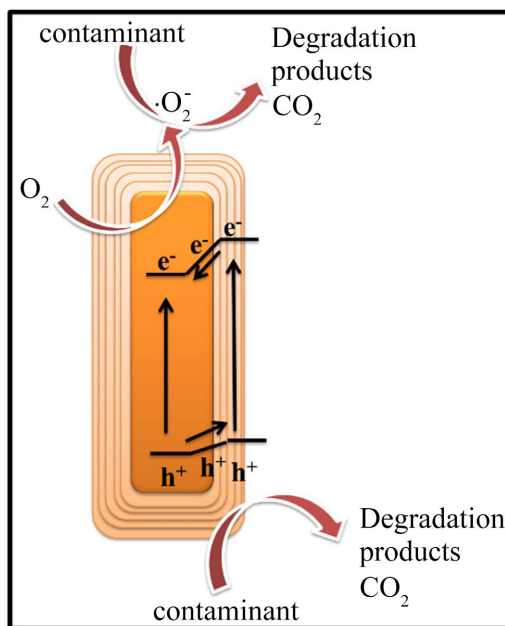


Figure 13. Possible mechanism for photocatalytic degradation of organics over β -AgVO₃/mpg-C₃N₄ [β -AgVO₃ rods (gold-orange) and mpg-C₃N₄ sheets (wheat brown)].

alignment of the polymer plains to the β -AgVO₃ surface facilitates the migration of electron-hole pairs formed in the layers of the mpg-C₃N₄, because the electron-migration proceeds via hopping perpendicular to the 2D layer planes and move directly to the surface. The improved long-range order of the optical tri-s-triazine units in the 2D mesoscopic polymer matrix, achieved by alignment at the crystal faces of the nanorod core, enhances markedly the charge carrier mobility [70] [71] [72]. Additionally, the small layer thickness *ca.* 7 - 11 nm, *i.e.* *ca.* 20 - 30 polymer planes enhances the migrations of excitons to the surface. Generally, the porosity and high specific surface area of the catalyst improves further the accessibility of active sites and the mass transfer of pollutants and degradation products. The holes are directly involved in the oxidation of the pollutants, e.g. hydroxylation of side chains and aromatic rings, and the cleavage of the aromatic ring. Superoxide radicals are formed by reduction of oxygen by conduction band electrons $O_2 + e_{(CB)}^- \rightarrow O_2^{\cdot-}$ and $O_2^{\cdot-} + H^+ \rightarrow HO_2^{\cdot}$. They then complete the total oxidation of organics to carbon dioxide and water.

4. Conclusion

β -AgVO₃/mpg-C₃N₄ composite catalysts of different compositions were prepared by soft mechanical mixing/milling in a mortar. The obtained composites were photocatalytic active in the degradation of ibuprofen under UV and visible room light irradiation. The photocatalytic activity was markedly higher compared to the single components and the highest activity was found with 20% β -AgVO₃/C₃N₄, specifically under room light irradiation. The superior activity results from the core/shell structure of this material which boosts photocatalytic degradation.

The TEM images of 20% to 30% loading of β -AgVO₃ show the realistic core/shell structures of the β -AgVO₃/C₃N₄ materials. Finally, an increase of the photocatalytic activity by a factor of 20 was noted with the core/shell catalyst compared to the single mp-g-C₃N₄, while the composite structures were less active and exhibited an increase by 9 times. Scavenger experiments have proved that valence band holes and anionic superoxide radicals are active species, and time-resolved photoluminescence measurements have proved increased mobility of the charge carriers in the carbonitrides. The latter leads to more effective charge separation, which is partially responsible for the increased catalytic efficiency.

Acknowledgements

This work was supported by the European Union in the frame of the FP7 program (EU-project PCATDES). We are very grateful to Dr. U. Bentrup (LIKAT) for diffuse reflectance UV-Vis measurements. We also thank Dr. Ch. Fischer (LIKAT) for ESI-TOF-MS measurements and Mrs. P. Duncker for TOC analysis.

Conflicts of Interest

The authors declare no conflicts of interest regarding the publication of this paper.

References

- [1] Choina, J., Kosslick, H., Fischer, C., Flechsig, G.U., Frunza, L. and Schulz, A. (2013) Photocatalytic Decomposition of Pharmaceutical Ibuprofen Pollutions in Water over Titania Catalyst. *Applied Catalysis B: Environmental*, **129**, 589-598. <https://doi.org/10.1016/j.apcatb.2012.09.053>
- [2] Xing, J., Fang, W.Q., Zhao, H.J. and Yang, H.G. (2012) Inorganic Photocatalysts for Overall Water Splitting. *Chemistry: An Asian Journal*, **7**, 642-657. <https://doi.org/10.1002/asia.201100772>
- [3] Habisreutinger, S.N., Schmidt-Mende, L. and Stolarczyk, J.K. (2013) Photocatalytic Reduction of CO₂ on TiO₂ and Other Semiconductors. *Angewandte Chemie International Edition*, **52**, 7372-7408. <https://doi.org/10.1002/anie.201207199>
- [4] Xuan, J. and Xiao, W.J. (2012) Visible-Light Photoredox Catalysis. *Angewandte Chemie International Edition*, **51**, 6828-6838. <https://doi.org/10.1002/anie.201200223>
- [5] Ismail, A.A. and Bahnemann, D.W. (2014) Photochemical Splitting of Water for Hydrogen Production by Photocatalysis: A Review. *Solar Energy Materials & Solar Cells*, **128**, 85-101. <https://doi.org/10.1016/j.solmat.2014.04.037>
- [6] Choina, J., Fischer, C., Flechsig, G.U., Kosslick, H., Tuan, V.A., Tuyen, N.D., Tuyen, N.A. and Schulz, A. (2014) Photocatalytic Properties of Zr-Doped Titania in the Degradation of the Pharmaceutical Ibuprofen. *Journal of Photochemistry and Photobiology A: Chemistry*, **274**, 108-116. <https://doi.org/10.1016/j.jphotochem.2013.08.018>
- [7] Hoffmann, M.R., Martin, S.T., Choi, W.Y. and Bahnemann, D.W. (1995) Environmental Applications of Semiconductor Photocatalysis. *Chemical Reviews*, **95**, 69-96.

- <https://doi.org/10.1021/cr00033a004>
- [8] Mori, K., Yamashita, H. and Anpo, M. (2012) Photocatalytic Reduction of CO₂ with H₂O on Various Titanium Oxide Photocatalysts. *RSC Advances*, **2**, 3165-3172. <https://doi.org/10.1039/c2ra01332k>
- [9] Liu, G., Zhao, Y.N., Sun, C.H., Li, F., Lu, G. and Wang, H.M. (2008) Synergistic Effects of B/N Doping on the Visible-Light Photocatalytic Activity of Mesoporous TiO₂. *Angewandte Chemie International Edition*, **47**, 4516-4520. <https://doi.org/10.1002/anie.200705633>
- [10] Pelaez, M., Nolan, N.T., Pillai, S.C., Seery, M.K., Falaras, P., Kontos, A.G., Dunlop, P.S.M., Hamilton, J.W.J., Byrne, J.A., O'Shea, K., Entezari, M.H. and Dionysiou, D.D. (2012) A Review on the Visible Light Active Titanium Dioxide Photocatalysts for Environmental Applications. *Applied Catalysis B: Environmental*, **125**, 331-349. <https://doi.org/10.1016/j.apcatb.2012.05.036>
- [11] Hara, M., Hitoki, G., Takata, T., Kondo, J.N., Kobayashi, H. and Domen, K. (2003) TaON and Ta₃N₅ as New Visible Light Driven Photocatalysts. *Catalysis Today*, **78**, 555-560. [https://doi.org/10.1016/S0920-5861\(02\)00354-1](https://doi.org/10.1016/S0920-5861(02)00354-1)
- [12] Wang, Y.J., He, Y.M., Li, T.T. and Cai, J. (2012) Novel CaBi₆O₁₀ Photocatalyst for Methylene Blue Degradation under Visible Light Irradiation. *Catalysis Communications*, **18**, 161-164. <https://doi.org/10.1016/j.catcom.2011.12.011>
- [13] Li, T.T., Wang, Y.J., He, Y.M., Cai, J., Luo, M.F. and Zhao, L.H. (2012) Preparation and Photocatalytic Property of Sr_{0.25}Bi_{0.75}O_{1.36} Photocatalyst. *Materials Letters*, **74**, 170-172. <https://doi.org/10.1016/j.matlet.2012.01.078>
- [14] Bi, Y., Ouyang, S., Umezawa, N., Cao, J. and Ye, J. (2011) Facet Effect of Single-Crystalline Ag₃PO₄ Sub-Microcrystals on Photocatalytic Properties. *Journal of the American Chemical Society*, **133**, 6490-6492. <https://doi.org/10.1021/ja200213z>
- [15] Shang, M., Wang, W.Z., Zhou, L., Sun, S.M. and Yin, W.Z. (2009) Nanosized BiVO₄ with High Visible-Light-Induced Photocatalytic Activity: Ultrasonic-Assisted Synthesis and Protective Effect of Surfactant. *Journal of Hazardous Materials*, **172**, 338-344. <https://doi.org/10.1016/j.jhazmat.2009.07.017>
- [16] Huang, C.M., Cheng, K.W., Pan, G.T., Chang, W.S. and Yang, T.C.K. (2010) CTAB-Assisted Hydrothermal Synthesis of Silver Vanadates and Their Photocatalytic Characterization. *Chemical Engineering Science*, **65**, 148-152. <https://doi.org/10.1016/j.ces.2009.03.022>
- [17] Mao, C., Wu, X.C., Zhu, J.J., Mao, C., Wu, X.C. and Zhu, J.J. (2008) Large Scale Preparation of β-AgVO₃ Nanowires Using a Novel Sonochemical Route. *Journal of Nanoscience and Nanotechnology*, **8**, 3203-3207.
- [18] Liu, S.W., Wang, W.Z., Zhou, L. and Zhang, L.S. (2006) Silver Vanadium Oxides Nanobelts and Their Chemical Reduction to Silver Nanobelts. *Journal of Crystal Growth*, **293**, 404-408. <https://doi.org/10.1016/j.jcrysgro.2006.05.045>
- [19] Li, G.C., Chao, K., Ye, C.S. and Peng, H.R. (2008) One-Step Synthesis of Ag Nanoparticles Supported on AgVO₃ Nanobelts. *Materials Letters*, **62**, 735-738. <https://doi.org/10.1016/j.matlet.2007.06.046>
- [20] Kittaka, S., Nishida, S. and Ohtani, T. (2002) Mechanochemical Reactions between Ag₂O and V₂O₅ to Form Crystalline Silver Vanadates. *Journal of Solid State Chemistry*, **169**, 139-142. [https://doi.org/10.1016/S0022-4596\(02\)00037-3](https://doi.org/10.1016/S0022-4596(02)00037-3)
- [21] Liang, S.Q., Zhou, J., Pan, A.Q., Li, Y.J., Chen, T., Tian, Z.M. and Ding, H.B. (2012) Facile Synthesis of β-AgVO₃ Nanorods as Cathode for Primary Lithium Batteries. *Materials Letters*, **74**, 176-179. <https://doi.org/10.1016/j.matlet.2012.01.101>
- [22] Zhou, J., Liang, Q., Pan, A.Q., Zhang, X.L., Zhu, Q.Y., Liang, S.Q. and Cao, G.Z.

- (2014) The General Synthesis of Ag Nanoparticles Anchored on Silver Vanadium Oxides: Towards High Performance Cathodes for Lithium-Ion Batteries. *Journal of Materials Chemistry A*, **2**, 11029-11034. <https://doi.org/10.1039/C4TA00437J>
- [23] Hu, X.X., Hu, C. and Qu, J.H. (2008) Preparation and Visible-Light Activity of Silver Vanadate for the Degradation of Pollutants. *Materials Research Bulletin*, **43**, 2986-2997. <https://doi.org/10.1016/j.materresbull.2007.11.022>
- [24] Wang, G., Ren, Y., Zhou, G.J., Wang, J.P., Cheng, H.F., Wang, Z.Y., Zhan, J., Huang, B.B. and Jiang, M.H. (2013) Synthesis of Highly Efficient Visible Light Ag@Ag₃VO₄ Plasmonic Photocatalysts. *Surface and Coatings Technology*, **228**, S283-S286. <https://doi.org/10.1016/j.surfcoat.2012.05.124>
- [25] Dolgos, M.R., Paraskos, A.M., Stoltzfus, M.W., Yarnell, S.C. and Woodward, P.M. (2009) The Electronic Structures of Vanadate Salts: Cation Substitution as a Tool for Band Gap Manipulation. *Journal of Solid State Chemistry*, **182**, 1964-1971. <https://doi.org/10.1016/j.jssc.2009.04.032>
- [26] Zhu, Y.P., Ren, T.Z. and Yuan, Z.Y. (2015) Mesoporous Phosphorus-Doped g-C₃N₄ Nanostructured Flowers with Superior Photocatalytic Hydrogen Evolution Performance. *ACS Applied Materials & Interfaces*, **7**, 16850-16856. <https://doi.org/10.1021/acsami.5b04947>
- [27] Zhu, K.X., Wang, W.J., Meng, A., Zhao, M., Wang, J.H., Zhao, M., Zhang, D.L., Jia, Y.P., Xu, C.H. and Li, Z.J. (2015) Mechanically Exfoliated g-C₃N₄ Thin Nanosheets by Ball Milling as High Performance Photocatalysts. *RSC Advances*, **5**, 56239-56243. <https://doi.org/10.1039/C5RA09040G>
- [28] Zhou, Y.J., Zhang, L.X., Liu, J.J., Fan, X.Q., Wang, B.Z., Wang, M., Ren, W.C., Wang, J., Li, M.L. and Shi, J.L. (2015) Brand New P-Doped g-C₃N₄: Enhanced Photocatalytic Activity for H₂ Evolution and Rhodamine B Degradation under Visible Light. *Journal of Materials Chemistry A*, **3**, 3862-3867. <https://doi.org/10.1039/C4TA05292G>
- [29] Wang, X.L., Fang, W.Q., Yao, Y.F., Liu, P.R., Wang, Y., Zhang, H.M., Zhao, H.J. and Yang, H.G. (2015) Switching the Photocatalytic Activity of g-C₃N₄ by Homogenous Surface Chemical Modification with Nitrogen Residues and Vacancies. *RSC Advances*, **5**, 21430-21433. <https://doi.org/10.1039/C5RA00150A>
- [30] Niu, P., Yin, L.C., Yang, Y.Q., Liu, G. and Cheng, H.M. (2014) Increasing the Visible Light Absorption of Graphitic Carbon Nitride (Melon) Photocatalysts by Homogeneous Self-Modification with Nitrogen Vacancies. *Advanced Materials*, **26**, 8046-8052. <https://doi.org/10.1002/adma.201404057>
- [31] Perera, D., Lorek, R., Khnayzer, R.S., Moroz, P., O'Connor, T., Khon, D., Diederich, G., Kinder, E., Lambright, S., Castellano, F.N. and Zamkov, M. (2012) Photocatalytic Activity of Core/Shell Semiconductor Nanocrystals Featuring Spatial Separation of Charges. *The Journal of Physical Chemistry C*, **116**, 22786-22793. <https://doi.org/10.1021/jp308921s>
- [32] Mitsudome, T. and Kaneda, K. (2013) Advanced Core-Shell Nanoparticle Catalysts for Efficient Organic Transformations. *ChemCatChem*, **5**, 1681-1691. <https://doi.org/10.1002/cctc.201200724>
- [33] Bai, X.J., Zong, R.L., Li, C.X., Liu, D., Liu, Y.F. and Zhu, Y.F. (2014) Enhancement of Visible Photocatalytic Activity via Ag@C₃N₄ Core-Shell Plasmonic Composite. *Applied Catalysis B: Environmental*, **147**, 82-91. <https://doi.org/10.1016/j.apcatb.2013.08.007>
- [34] Zhu, T.T., Song, Y.H., Ji, H.Y., Xu, Y.G., Song, Y.X., Xia, J.X., Yin, S., Li, Y.P., Xu, H., Zhang, Q. and Li, H.M. (2015) Synthesis of g-C₃N₄/Ag₃VO₄ Composites with

- Enhanced Photocatalytic Activity under Visible Light Irradiation. *Chemical Engineering Journal*, **271**, 96-105. <https://doi.org/10.1016/j.cej.2015.02.018>
- [35] Kumar, S., Surendar, T., Baruah, A. and Shanker, V. (2013) Synthesis of a Novel and Stable g-C₃N₄-Ag₃PO₄ Hybrid Nanocomposite Photocatalyst and Study of the Photocatalytic Activity under Visible Light Irradiation. *Journal of Materials Chemistry A*, **1**, 5333-5340. <https://doi.org/10.1039/c3ta00186e>
- [36] Xu, H., Yan, J., Xu, Y., Song, Y., Li, H., Xia, J., Huang, C., and Wan, H. (2013) Novel Visible-Light-Driven AgX/Graphite-Like C₃N₄ (X = Br, I) Hybrid Materials with Synergistic Photocatalytic Activity. *Applied Catalysis B: Environmental*, **129**, 182-193. <https://doi.org/10.1016/j.apcatb.2012.08.015>
- [37] Li, T.T., Zhao, L.H., He, Y.M., Cai, J., Luo, M.F. and Lin, J.J. (2013) Synthesis of g-C₃N₄/SmVO₄ Composite Photocatalyst with Improved Visible Light Photocatalytic Activities in RhB Degradation. *Applied Catalysis B: Environmental*, **129**, 255-263. <https://doi.org/10.1016/j.apcatb.2012.09.031>
- [38] He, Y.M., Cai, J., Zhang, L.H., Wang, X.X., Lin, H.J., Teng, B.T., Zhao, L.H., Weng, W.Z., Wan, H.L. and Fan, M.H. (2014) Comparing Two New Composite Photocatalysts, *t*-LaVO₄/g-C₃N₄ and *m*-LaVO₄/g-C₃N₄, for Their Structures and Performances. *Industrial & Engineering Chemistry Research*, **53**, 5905-5915. <https://doi.org/10.1021/ie4043856>
- [39] He, Y.M., Cai, J., Li, T.T., Wu, Y., Lin, H.J., Zhao, L.H. and Luo, M.F. (2013) Efficient Degradation of RhB over GdVO₄/g-C₃N₄ Composites under Visible-Light Irradiation. *Chemical Engineering Journal*, **215**, 721-730. <https://doi.org/10.1016/j.cej.2012.11.074>
- [40] Shen, K., Gondal, M.A., Siddique, R.G., Shi, S., Wang, S.Q., Sun, J.B. and Xu, Q.Y. (2014) Preparation of Ternary Ag/Ag₃PO₄/g-C₃N₄ Hybrid Photocatalysts and Their Enhanced Photocatalytic Activity Driven by Visible Light. *Chinese Journal of Catalysis*, **35**, 78-84. [https://doi.org/10.1016/S1872-2067\(12\)60712-8](https://doi.org/10.1016/S1872-2067(12)60712-8)
- [41] Zhao, W., Guo, Y., Wang, S.M., He, H., Sun, C. and Yang, S.G. (2015) A Novel Ternary Plasmonic Photocatalyst: Ultrathin g-C₃N₄ Nanosheet Hybridized by Ag/AgVO₃ Nanoribbons with Enhanced Visible-Light Photocatalytic Performance. *Applied Catalysis B: Environmental*, **165**, 335-343. <https://doi.org/10.1016/j.apcatb.2014.10.016>
- [42] Chen, Y.F., Huang, W.X., He, D.L., Yue, S.T. and Huang, H. (2014) Construction of Heterostructured g-C₃N₄/Ag/TiO₂ Microspheres with Enhanced Photocatalysis Performance under Visible-Light Irradiation. *ACS Applied Materials & Interfaces*, **6**, 14405-14414. <https://doi.org/10.1021/am503674e>
- [43] Yan, H. (2012) Soft-Templating Synthesis of Mesoporous Graphitic Carbon Nitride with Enhanced Photocatalytic H₂ Evolution under Visible Light. *Chemical Communications*, **48**, 3430-3432. <https://doi.org/10.1039/c2cc00001f>
- [44] Murphy, A.B. (2007) Band-Gap Determination from Diffuse Reflectance Measurements of Semiconductor Films, and Application to Photoelectrochemical Water-Splitting. *Solar Energy Materials & Solar Cells*, **91**, 1326-1337. <https://doi.org/10.1016/j.solmat.2007.05.005>
- [45] Murphy, A.B. (2007) Optical Properties of an Optically Rough Coating from Inversion of Diffuse Reflectance Measurements. *Applied Optics*, **46**, 3133-3143. <https://doi.org/10.1364/AO.46.003133>
- [46] Weckhuysen, B.M. and Schoonheydt, R.A. (1999) Recent Progress in Diffuse Reflectance Spectroscopy of Supported Metal Oxide Catalysts. *Catalysis Today*, **49**, 441-451. [https://doi.org/10.1016/S0920-5861\(98\)00458-1](https://doi.org/10.1016/S0920-5861(98)00458-1)

- [47] Kubelka, P. and Munk, F.Z. (1931) Ein Beitrag zur Optik der Farbabstriche. *Technical Physics*, **12**, 539-601.
- [48] Kubelka, P. (1948) New Contributions to the Optics of Intensely Light-Scattering Materials. Part I. *Journal of the Optical Society of America*, **38**, 448-457. <https://doi.org/10.1364/JOSA.38.000448>
- [49] Wang, Y., Ibad, M.F., Kosslick, H., Harloff, J., Beweries, T., Radnik, J., Schulz, A., Tschierlei, S., Lochbrunner, S. and Guo, X. (2015) Impact of the Crystallinity of Mesoporous Polymeric Graphitic Carbon Nitride on the Photocatalytic Performance under UV and Visible Light. *Microporous and Mesoporous Materials*, **211**, 182-191. <https://doi.org/10.1016/j.micromeso.2015.02.050>
- [50] Fina, F., Cellaar, S.K., Carins, G.M. and Irvine, T.S. (2015) Structural Investigation of Graphitic Carbon Nitride via XRD and Neutron Diffraction. *Chemistry of Materials*, **27**, 2612-2618. <https://doi.org/10.1021/acs.chemmater.5b00411>
- [51] Sediri, F. and Gharbi, N. (2009) Controlled Hydrothermal Synthesis of VO₂(B) Nanobelts. *Materials Letters*, **63**, 15-18. <https://doi.org/10.1016/j.matlet.2008.08.022>
- [52] Frost, R.L., Erickson, K.L., Weier, M.L. and Carmody, O. (2005) Raman and Infrared Spectroscopy of Selected Vanadates. *Spectrochimica Acta Part A: Molecular and Biomolecular Spectroscopy*, **61**, 829-834. <https://doi.org/10.1016/j.saa.2004.06.006>
- [53] Su, Q., Huang, C.K., Wang, Y., Fan, Y.C., Lu, B.A., Lan, W., Wang, Y.Y. and Liu, X.Q. (2009) Formation of Vanadium Oxides with Various Morphologies by Chemical Vapor Deposition. *Journal of Alloys and Compounds*, **475**, 518-523. <https://doi.org/10.1016/j.jallcom.2008.07.078>
- [54] Liu, H.W. and Tang, D.G. (2009) Synthesis of ZnV₂O₆ Powder and Its Cathodic Performance for Lithium Secondary Battery. *Materials Chemistry and Physics*, **114**, 656-659. <https://doi.org/10.1016/j.matchemphys.2008.10.055>
- [55] Souza, A.G., Ferreira, O.P., Santos, E.J.G., Mendes, J. and Alves, O.L. (2004) Raman Spectra in Vanadate Nanotubes Revisited. *Nano Letters*, **4**, 2099-2104. <https://doi.org/10.1021/nl0488477>
- [56] Holtz, R.D., Souza Filho, A.G., Brocchi, M., Martins, D., Duran, N. and Alves, O.L. (2010) Acetonitrile Mediated Facile Synthesis and Self-Assembly of Silver Vanadate Nanowires into 3D Spongy-Like Structure as a Cathode Material for Lithium Ion Battery. *Nanotechnology*, **21**, 185102-185110. <https://doi.org/10.1088/0957-4484/21/18/185102>
- [57] Wang, C.B., Deo, G. and Wachs, I.E. (1999) Interaction of Polycrystalline Silver with Oxygen, Water, Carbon Dioxide, Ethylene, and Methanol: *In Situ* Raman and Catalytic Studies. *The Journal of Physical Chemistry B*, **103**, 5645-5656. <https://doi.org/10.1021/jp984363l>
- [58] Baran, E.J. (1997) Vibrational Spectra of Ba₂(VO)₂O₈. *Journal of Raman Spectroscopy*, **28**, 289-291. [https://doi.org/10.1002/\(SICI\)1097-4555\(199704\)28:4<289::AID-JRS106>3.0.CO;2-4](https://doi.org/10.1002/(SICI)1097-4555(199704)28:4<289::AID-JRS106>3.0.CO;2-4)
- [59] Popovic, Z.V., Konstantinovic, M.J., Moshchalkov, V.V., Isobe, M. and Ueda, Y.J. (2003) Raman Scattering Study of Charge Ordering in β -Ca_{0.33}V₂O₅. *Journal of Physics: Condensed Matter*, **15**, L139-L145. <https://doi.org/10.1088/0953-8984/15/6/101>
- [60] Wallington, T.J., Egsgaard, H., Nielsen, O.J., Platz, J., Sehested, J. and Stein, T. (1998) Raman Scattering Study of Charge Ordering in β -Ca_{0.33}V₂O₅. *Chemical Physics Letters*, **290**, 363-370. [https://doi.org/10.1016/S0009-2614\(98\)00537-5](https://doi.org/10.1016/S0009-2614(98)00537-5)
- [61] Shi, H., Zhang, C. and Zhou, C. (2015) g-C₃N₄ Hybridized with AgVO₃ Nanowires: Preparation and Its Enhanced Visible-Light-Induced Photocatalytic Activity. *RSC*

- Advances*, **5**, 50146-50154. <https://doi.org/10.1039/C5RA08367B>
- [62] Serpone, N., Texier, I., Emeline, A.V., Pichat, P., Hidaka, H. and Zhao, J. (2000) Post-Irradiation Effect and Reductive Dechlorination of Chlorophenols at Oxygen-free TiO₂/Water Interfaces in the Presence of Prominent Hole Scavengers. *Journal of Photochemistry and Photobiology A: Chemistry*, **136**, 145-155. [https://doi.org/10.1016/S1010-6030\(00\)00348-8](https://doi.org/10.1016/S1010-6030(00)00348-8)
- [63] Minero, C., Mariella, G., Maurino, V. and Pelizzetti, E. (2000) The Fate of Organic Nitrogen in Photocatalysis: An Overview. *Langmuir*, **16**, 2632-2641. <https://doi.org/10.1021/la9903301>
- [64] Minero, C., Mariella, G., Maurino, V., Vione, D. and Pelizzetti, E. (2000) Photocatalytic Transformation of Organic Compounds in the Presence of Inorganic Ions. 2. Competitive Reactions of Phenol and Alcohols on a Titanium Dioxide-Fluoride System. *Langmuir*, **16**, 8964-8972. <https://doi.org/10.1021/la0005863>
- [65] Hollmann, D., Karnahl, M., Tschierlei, S., Kailasam, K., Schneider, M., Radnik, J., Grabow, K., Bentrup, U., Junge, H., Beller, M., Lochbrunner, S., Thomas, A. and Brückner, A. (2014) Structure-Activity Relationships in Bulk Polymeric and Sol-Gel-Derived Carbon Nitrides during Photocatalytic Hydrogen Production. *Chemistry of Materials*, **26**, 1727-1733. <https://doi.org/10.1021/cm500034p>
- [66] Zhang, H. and Yu, A. (2014) Photophysics and Photocatalysis of Carbon Nitride Synthesized at Different Temperatures. *The Journal of Physical Chemistry C*, **118**, 11628-11635. <https://doi.org/10.1021/jp503477x>
- [67] Merschjann, C., Tyborski, T., Orthmann, S., Yang, F., Schwarzburg, K., Lublow, M., Lux-Steiner, M.C. and Schedel-Niedrig, T. (2013) Photophysics of Polymeric Carbon Nitride: An Optical Quasimonomer. *Physical Review B*, **87**, 205204-205212. <https://doi.org/10.1103/PhysRevB.87.205204>
- [68] Merschjann, C., Tschierlei, S., Tyborski, T., Kailasam, K., Orthmann, S., Hollmann, D., Schedel-Niedrig, T., Thomas, A. and Lochbrunner, S. (2015) Complementing Graphenes: 1D Interplanar Charge Transport in Polymeric Graphitic Carbon Nitrides. *Advanced Materials*, **27**, 7993-7999. <https://doi.org/10.1002/adma.201503448>
- [69] Ung Thi Dieu Thuy, Nguyen Quang Liem, Parlett, Ch.M.A., Lalev, G.M. and Wilson, K. (2014) Synthesis of CuS and CuS/ZnS Core/Shell Nanocrystals for Photocatalytic Degradation of Dyes under Visible Light. *Catalysis Communications*, **44**, 62-67. <https://doi.org/10.1016/j.catcom.2013.07.030>
- [70] Sata, N., Eberman, K., Eberl, K. and Maier, J. (2000) Mesoscopic Fast Ion Conduction in Nanometre-Scale Planar Heterostructures. *Nature*, **408**, 946-949. <https://doi.org/10.1038/35050047>
- [71] Maier, A., Löffler, R. and Scheele, M. (2020) Fabrication of Nanocrystal Superlattice Microchannels by Soft-Lithography for Electronic Measurements of Single-Crystalline Domains. *Nanotechnology*, **31**, 405302-405313. <https://doi.org/10.1088/1361-6528/ab9c52>
- [72] Maier, A., Lapkin, D., Mukaramova, N., *et al.* (2020) Structure-Transport Correlation Reveals Anisotropic Charge Transport in Coupled PbS Nanocrystal Superlattices. *Advanced Materials*, **32**, Article ID: 2002254. <https://doi.org/10.1002/adma.202002254>